Experimental and numerical investigation of the Refined Zigzag Theory for accurate buckling analysis of highly heterogeneous sandwich beams

International Journal of Structural Stability and Dynamics

Experimental and numerical investigation of the Refined Zigzag Theory for accurate buckling analysis of highly heterogeneous sandwich beams

Alessia Ascione*

School of Engineering, RMIT University, GPO Box 2476 Melbourne, Victoria 3000, Australia
Department of Mechanical and Aerospace Engineering, Politecnico di Torino,
Corso Duca degli Abruzzi 24 Torino, 10129, Italy
alessia.ascione@polito.it

Adrian Cirino Orifici

School of Engineering, RMIT University, GPO Box 2476
Melbourne, Victoria 3000, Australia
adrian.orifici@rmit.edu.au

Marco Gherlone

Department of Mechanical and Aerospace Engineering, Politecnico di Torino,
Corso Duca degli Abruzzi 24 Torino, 10129, Italy
marco.gherlone@polito.it

Received (Day Month Year)
Accepted (Day Month Year)

The Refined Zigzag Theory (RZT) is a structural theory developed for the analysis of composite multilayer and sandwich beams. However, the accuracy of RZT for buckling analysis of sandwich beams has not been experimentally investigated, and for RZT and Timoshenko Beam Theory (TBT) the effect of the degree of heterogeneity on their accuracy requires further study. The aim of this work was to validate the use of the RZT for predicting the critical buckling loads of sandwich beams, even with highly heterogeneous material properties, and to assess the use of the TBT for the same application. Buckling experiments were conducted on five foam-core sandwich beams, which varied in geometry and included highly heterogeneous configurations. For each beam, two finite element models were analysed using RZT- and TBT-beam finite elements. The comparison between the numerical and the experimental results highlighted a major capability of RZT to correctly predict the critical buckling load for all the beams considered. The dependance of the TBT results on the beam characteristics was further investigated through a parametric analysis, which showed the dominant effect to be a close to linear relationship between the TBT error and the beam face-to-core thickness ratio. The work demonstrated the outstanding accuracy of the RZT predictions, including the superior capabilities with respect to TBT, and has application for rapid and accurate analysis of industrial structures.

Keywords: Refined Zigzag Theory, Sandwich beams, Buckling experiments, Geometric nonlinearities, Southwell method.

*Corresponding author.

1. Introduction

Sandwich structures are widely used for lightweight constructions in mechanical, naval, civil and aerospace engineering applications. The reasons for their success are the attractive properties of high stiffness, light weight and high energy absorption capability. A sandwich structure consists of two thin and high-strength material facesheets, bonded to a thick core made of a lightweight material such as a metallic honeycomb or a structural foam. Metallic honeycombs have a high shear modulus and high compressive strength, whereas foam-core sandwiches can be more convenient for their lower manufacturing cost and time due to a simpler production process.

In aerospace applications, the compression resistance of shell structures is increased by means of stiffening profiles, called stringers, bonded to the shells. Some aircraft designs involve the usage of polymethacrylimide (PMI) foams to fill the area between the stringer and the shell, and one application of foam-filled stringers is for the rear pressure bulkhead of the Airbus A340, the A340-600 and the A380.[1] One advantage of foam-filled hat-stringers with respect to their hollow configuration is the significant improvement of the buckling resistance, which avoids the premature failure due to the side wall buckling, typical of the hollow stringers.[2]

In structural analysis, stringers are usually modelled as beams. Depending on their application, beam structures carry various types of load like bending and transverse-shear loads, or axial tensile and compressive loads. Researchers have extensively investigated the static bending response, the buckling behaviour and the free-vibrations of beams, both numerically and through experiments. The theories most commonly used for the analysis of beams are the classical Bernoulli-Euler (BE) beam theory and the Timoshenko Beam Theory (TBT).[3,4] The Bernoulli-Euler beam theory is based on the assumption of negligible transverse-shear deformations and it is generally accurate only for slender beams, even when made of homogenous materials. TBT takes into account also the transverse-shear deformation, thus it is more accurate than BE for beams with low slenderness ratios, but a shear correction factor is required to correct the hypothesis of constant transverse-shear strain through the beam thickness. Nevertheless, both BE and TBT cannot represent the complex distribution of the in-plane displacement across the thickness of a composite beam. They assume that the beam cross-section remains planar after the deformation whereas, for composite beams, the derivative of the axial displacement with respect to the thickness coordinate is usually discontinuous at the interface between two consecutive layers. For this reason, BE and TBT can lead to significantly erroneous results in the prediction of the strains and stresses of composite laminated and sandwich beams. Frostig et al.[5] pointed out that the assumption of a planar transversal section after the deformation was not true especially for sandwich beams with a foam core or a low-strength honeycomb core. They developed a higher-order theory for the analysis of soft-core sandwich beams taking into account the core vertical flexibility, which was negligible for the stiff metallic honeycombs.

The theory proposed by Frostig et al. considered the skins as two ordinary thin beams with axial and bending resistance, whereas the core was a two-dimensional elastic medium with a transverse shear resistance only. They employed the theory also for the buckling analysis of soft-core sandwich beams.[6]

A more general approach to reproduce the nonlinear trend of the in-plane displacement across the thickness of composite laminated and sandwich beams is to increase the order of the truncated power series expansion used to express the displacement field component as a function of the thickness variable. The theories developed in this way are called High-order Shear Deformation Theories (HSDTs), or Equivalent Single Layer (ESL) theories because one displacement field is assumed for the entire laminate (one single series expansion for each displacement component of the entire laminate). Khedir and Reddy employed a third-order shear deformation theory for the bending,[7] the buckling[8] and the free-vibration[9] analysis of cross-ply laminated beams with various boundary conditions. Ramos Loja et al. used a higher order shear deformation theory to develop a finite element formulation for the static and dynamic analysis of multilayer composite beams.[10] However in the HSDTs, the in-plane displacement component is a function of differentiability class higher than zero, thus its through-the-thickness derivative is continuous at the layer interfaces, contradicting the actual behaviour of a beam made of different material layers.[11] Kahya[12] developed a finite element for the analysis of multilayer beams assuming the TBT kinematics for each layer in order to have a piecewise linear distribution of the in-plane displacement across the beam thickness. The kinematic formulation for the entire laminate could account for a discontinuous derivative of the in-plane displacement component across the thickness, but the resulting number of degrees of freedom was dependent on the number of layers. The same approach is followed by the Layer-Wise theories (LW), where a specific kinematics is chosen independently for each layer to guarantee a C^0 distribution of the in-plane displacement across the thickness.[13,14] The major drawback of the LW theories is the higher number of degrees of freedom than the HSDTs, which leads to a higher computational cost dependent on the number of layers. This is the reason why TBT is still one of the most used theories for the analysis of composite beams; it is used also for the finite elements of commercial codes because of the simplicity of the formulation and the low computational cost. However, even the adoption of a shear correction factor calculated specifically for each beam lamination does not make TBT sufficiently accurate for composite and sandwich beams in general, as for highly heterogeneous material laminations.[15]

The Zigzag (ZZ) theories are a subclass of the general LW theories developed to overcome the issue of a number of degrees of freedom depending on the number of layers. As in the HSDTs, the ZZ theories have a number of degrees of freedom independent of the number of layers, and they are also able to reproduce the piecewise-linear distribution of the in-plane displacement across the thickness, which makes them more suitable than the HSDTs for the analysis of beams with highly heterogeneous material laminations. The Zigzag models were pioneered by

Di Sciuva in the early eighties, with some of his works also concerning stability and buckling problems.[16] Di Sciuva's approach inspired many authors, especially those interested in sandwich structures like Khandelwal et al., who created a finite element based on a higher order zigzag theory for the vibration and buckling analysis of sandwich laminates with soft cores.[17]

More recently, Tessler, Di Sciuva and Gherlone developed the Refined Zigzag Theory (RZT),[18] which was proven to be superior to HDSTs for the analysis of composite and sandwich plates,[19] also functionally graded.[20] The RZT was successfully assessed for the analysis of foam-core sandwich beams and experiments were conducted to validate the theory for the static bending[21] and the free-vibration[22] analysis. The RZT was extended introducing the geometric nonlinearities for calculating the critical buckling loads of composite and sandwich plates[19] and both the geometric nonlinearities and geometric imperfections were considered in the formulation for the buckling and postbuckling analysis of composite and sandwich beams.[23] However, the RZT predictions of the critical buckling loads of composite and sandwich beams were just numerically verified through the comparison with highly detailed finite element models in commercial codes, and no experimental assessments were conduced to validate the use of the theory for these applications. Moreover, the comparison between the RZT predictions, the experiments and the results obtained by FE models based on TBT showed that both the TBT error with respect to the experimental data and the TBT deviation from the RZT results increased for sandwich beams with higher face-to-core thickness ratios and higher face-to-core stiffness ratios, highlighting some kind of dependence of the TBT error on the beam characteristics.[21,22,23] However, the correlation between the TBT error and the beam material and geometrical properties was not further investigated by the authors.

Various techniques are available for the experimental evaluation of the critical buckling load of beams. The Southwell method is the most used approach for static and non-destructive tests, where the critical buckling load is calculated from the values of the applied load, N_0, and the corresponding transversal displacement of the beam, w, recorded during the experiments.[24] The method approximates the load-displacement equilibrium path, obtained plotting N_0 as a function of w, as a rectangular hyperbola. Through a coordinate transformation, the hyperbola becomes a straight line in the $(w, \frac{w}{N_0})$ plane, which is called Southwell plot, and the slope of the line corresponds to the asymptotic load value of the hyperbola, i.e. the critical buckling load. Southwell developed his method for homogeneous beams, but later on it was also applied to composite beams.[25] In their experimental investigations, Chailleux et al. wanted to assess the usage of methods developed for homogeneous structures for the critical bucking load evaluation of composite columns and plates. They employed the Southwell method for columns in both simply-supported and clamped boundary conditions, but the comparison with theoretical predictions showed better results for the simply-supported cases, probably due to the difficulty of realising a perfect clamp. A concern about the boundary conditions to use for

buckling experiments was expressed by Singer et al., who recommended the use of simply-supported conditions rather than the clamped conditions for buckling tests performed to validate a new theory.[26] The reason is that the critical cross-section of a beam in simply-supported boundary conditions is at half the length of the beam, thus it is far less influenced by the ends; in addition, the effective length of a clamped beam is hard to determine because it is highly dependent on the restraining method. Many authors proposed modified versions of the Southwell method to account for particular boundary conditions and for beams with small geometric imperfections,[27,28] or to consider the effect of the small pre-load and deflection measured at the beginning of the experiment,[29] but the classical formulation remains the most used. Mandal et al. employed the Southwell method for the lateral-torsional buckling of beams, proving the superiority of the standard formulation compared to a modified form, where the square of the load was used in the Southwell plot rather than the load value itself.[30] The Southwell method was employed for the flexural and the lateral-torsional buckling of columns made of steel[31] and also laminated composite.[32,33,34] In other works, the method was applied to sandwich beams with a debonding between the foam-core and the facesheets, and the authors found that the critical buckling load decreased for lower values of the core density and for a higher length of debonding.[35,36]

In the present work, a numerical and an experimental investigation have been conducted to characterise the accuracy of finite element models based on RZT and TBT for the buckling analysis of sandwich beams. As highlighted above, the RZT represents a good compromise between the accuracy of the LW theories and the computational cost of the ESL theories, and it is also very precise for highly heterogeneous sandwich structures. On the other hand, TBT is not accurate enough in general, especially for sandwich beams with very soft cores or relatively thick facesheets. For this reason, five sandwich beams with different face-to-core stiffness ratios, obtained by using two different structural foams for the core, and various face-to-core thickness ratios have been tested for calculating the experimental critical buckling loads of the beams by employing the Southwell method. The experimental critical buckling loads have been taken as reference values for verifying the numerical predictions. Furthermore, the nonlinear formulation of the RZT[23] has been employed to realise the finite element models of the sandwich beams based on C^0 shape functions[37] and the critical buckling loads have been calculated as the first eigenvalue of the stability equation. The same approach has been used for calculating the critical buckling loads based on TBT finite elements. The results obtained by the two numerical models for each beam have been compared to identify the beams with the highest deviation of the RZT solution from TBT. Subsequently, the numerical results have been compared to the experimental critical buckling loads calculating the percentage error of the numerical solutions with respect to the experiments. The percentage error of the RZT has demonstrated the high accuracy of RZT in any case, whereas TBT has differed significantly from the experiments for the same beams. Hence, a further numerical investigation has

been carried out to determine the dependance of the TBT deviation from RZT on the beam geometric and material characteristics. The outcomes of this parametric study have shown a close to linear relationship between the TBT error and the face-to-core stiffness ratio and a higher-order dependance of the error on face-to-core thickness ratio.

This work provides the first experimental demonstration that RZT is able to predict the critical buckling load of sandwich beams with a high level of accuracy, independent of the beam characteristics including high heterogeneity. In addition, this work provides a new characterisation of the relationship between the error in TBT analysis and the beam material and geometrical properties, further highlighting the superiority of RZT with respect to TBT for the buckling analysis of sandwich beams.

2. Beam manufacture

Carbon fibre-reinforced polymer (CFRP) prepregs were used for making the facesheets of the sandwich beams, placing the prepreg layers in a cross-ply [0°/90°/90°/0°] configuration. Facesheets of various thicknesses were manufactured considering different numbers of prepreg layers for each orientation angle. The cross-ply layups were plates wider and longer than the final facesheets and they were cured in autoclave according to manufacturer specifications (1 hour, 120°C, 90 psi). Once cured, the plates were cut in the desired dimensions to make the facesheets. Two Rohacell® structural foams, the Rohacell®IG31 and the Rohacell®WF110, were used as the material for the core of the beams. The facesheets were bonded to the core using the 3M™ AF163-2K structural adhesive film, curing it in the autoclave. Fig.[1a] shows the vacuum bag for bonding the core to the facesheets, where the beams were surrounded by aluminium frames to prevent the foam from squashing under the vacuum or the autoclave pressure. After the curing, the sandwich beams were refined using a surface grinder to make the edges straight and parallel (see Fig.[1b]).

The final dimensions of the beams are indicated in Table [1]; the total length is L and the width, b, is approximately three times the total thickness, h, of the beam. The thickness of the facesheets, h_f, and the thickness of the core, h_c, were measured before bonding the core to the facesheets. The adhesive thickness, h_a, was calculated as the difference between the total thickness and the sum of the core and facesheet thicknesses.

A Keyence LC-2320 laser displacement meter sensor was used to measure the initial stress-free deflection of the beams. However, the order of magnitude of the detected values was small compared to the geometric tolerances considered for the specimens. The difference in the values detected by the laser along the beam length could be attributed to the small thickness variations of facesheets, core or adhesive rather than to the actual deviation of the beam centroidal axis from a straight configuration. Hence, the specimens were very close to a straight beam

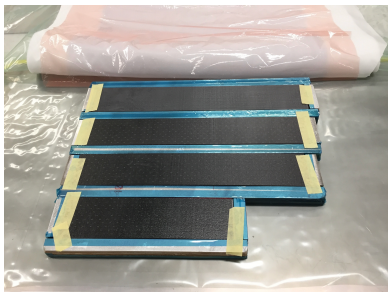

(a) Vacuum bag with aluminium frames for bonding the core to the facesheets.

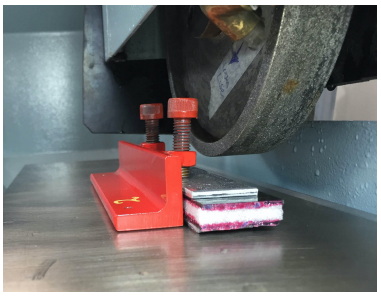

(b) Surface grinder used to refine the beam edges.

Fig. 1: Sandwich beams manufacturing.

Table 1: Geometrical properties of the beams.

Beam	**L** (mm)	**b** (mm)	$\mathbf{h_c}$ (mm)	$\mathbf{h_f}$ (mm)	$\mathbf{h_a}$ (mm)	$\mathbf{h_f/h_c}$ -	**L/h** -	**Facesheet ply orientation**
WF-1-L1	443	63.00	20.00	0.68	0.241	0.034	20.28	[0°/90°/90°/0°]
WF-1-L2	427	64.29	20.00	0.68	0.240	0.034	19.55	[0°/90°/90°/0°]
IG-2-L1	160	25.69	5.40	1.45	0.157	0.268	18.57	[0°/90°/90°/0°]
IG-4-L1	230	36.25	5.00	3.40	0.140	0.680	19.04	[0°/90°/90°/0°]
IG-4-L2	230	37.67	5.00	3.40	0.240	0.680	18.73	[0°/90°/90°/0°]

configuration.

Simply supported boundary conditions were realised by bonding cylindrical steel supports to the ends of each beam, as shown in Fig.[2a]. The epoxy adhesive used for the bonding was 3M^{TM} Scotch-Weld^{TM} DP460NS. In each case, the radius of the semi-cylinder, R_e, was equal to the nominal thickness of the beam, the width b_e was 4 mm wider than the beam width and the angle of the circular sector of the cylinder cross-sectional area was set to 140°, a value much higher than the expected rotations of the beams around the y-axis (refer to Fig.[2b]).

3. Numerical analysis based on RZT and TBT

In this section, the critical buckling load of each beam is calculated using two finite element models, one based on the Refined Zigzag Theory and one based on the Timoshenko Beam Theory. The basic assumptions of the RZT[18] and its application to the buckling analysis of composite and sandwich beams are reviewed before presenting the buckling loads calculated for the sandwich beams tested experimentally.[38]

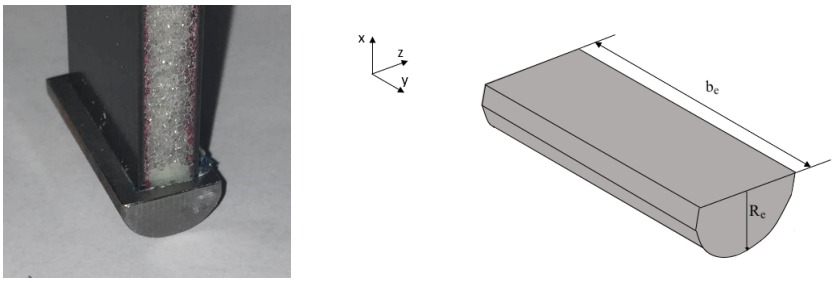

(a) Steel support bonded to a sandwich beam.

(b) Geometrical properties of the supports.

Fig. 2: Supports for simply-supported boundary conditions.

3.1. *RZT and finite element formulation for the buckling analysis*

A composite multilayer beam is oriented in the way that its longitudinal axis corresponds to the $x-$coordinate, $x \in [x_a, x_b]$, of a Cartesian coordinate system (x, y, z), with the $z-$axis, $z \in [-h, h]$, corresponding to the beam thickness, $2h$ (see Fig.[3]). The total length of the beam is L and the cross-sectional area $A = 2h \times b$ lays in the (y, z) plane. The beam lamination is constituted of N orthotropic material layers with the orthotropy axes corresponding to the Cartesian coordinates. The mechanical loads applied to the bottom ($z = -h$) and the top ($z = +h$) beam surfaces are the distributed axial loads, $p^b(x)$ and $p^t(x)$, and the distributed transverse loads, $q^b(x)$ and $q^t(x)$ (units of force/ length). In addition, the end cross-sections are subjected to the prescribed axial (T_{xa}, T_{xb}) and transverse-shear (T_{za}, T_{zb}) tractions. Only planar deformations in the (x, z) plane are considered under the assigned load system.

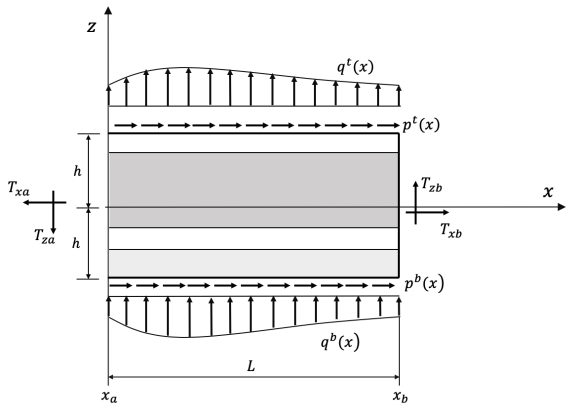

Fig. 3: Beam notation and applied loads.

The thickness of each layer is $2h^{(k)}$, where the superscript (k) refers to the kth material layer. A subscript $i = 0, 1, \cdots, N$ is used to indicate the interface between two consecutive layers; Fig.[4a] shows that $i = 0$ at the first interface layer, where $z \equiv z_{(0)} = -h$, and $i = N$ at the last interface, where $z \equiv z_{(N)} = h$.
The orthogonal displacement vector of the Refined Zigzag Theory is defined as

$$\mathbf{s} \equiv \begin{Bmatrix} u_x^{(k)}(x,z) \\ u_z(x,z) \end{Bmatrix} = \begin{bmatrix} 1 & 0 & z & \phi^{(k)} \\ 0 & 1 & 0 & 0 \end{bmatrix} \begin{Bmatrix} u(x) \\ w(x) \\ \theta(x) \\ \psi(x) \end{Bmatrix} \equiv \mathbf{Z_u u}\,, \tag{3.1}$$

where $u_x^{(k)}$ and u_z are the displacements in the directions of the $x-$ and the $z-$axis, respectively. The transverse displacement $u_z \equiv w$ is assumed to be uniform along the beam thickness, thus it is independent of the kth layer characteristics. The vector $\mathbf{u}$ contains the four kinematic variables of the theory: the uniform axial displacement, $u(x)$, the deflection, $w(x)$, the average cross-sectional (bending) rotation, $\theta(x)$, and the zigzag rotation, $\psi(x)$. The variable $\psi(x)$ is required for modelling the zigzag trend of the axial displacement function across the thickness. The total zigzag displacement is obtained multiplying $\psi(x)$ and the zigzag function, $\phi^{(k)}$. As highlighted in Fig.[4b], $\phi^{(k)}$ is C^0-continuous and piecewise linear across the beam thickness, vanishing on both the top and the bottom surfaces of the beam.

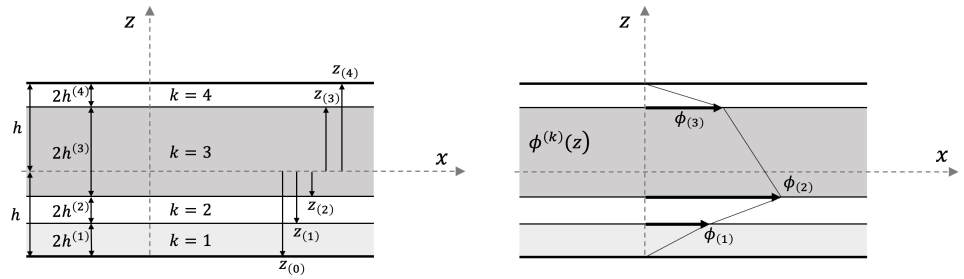

(a) Layer notation. (b) Zigzag function distribution.

Fig. 4: Through-the-thickness layer notation of the Refined Zigzag Theory for a four-layer beam.

The slope of the linear distribution of the zigzag function in each layer, $\beta^{(k)} \equiv \phi_{,z}^{(k)}$, depends on the thickness and on the transverse shear modulus of each layer, and it is piecewise constant along the thickness. $\beta^{(k)}$ can be calculated as follows:

$$\beta^{(k)} = \frac{G}{G_{xz}^{(k)}} - 1\,, \qquad k = 1, \cdots, N\,, \tag{3.2}$$

where $G_{xz}^{(k)}$ is the transverse-shear modulus of the kth layer and G is the quantity defined as

$$G = \frac{2h}{\sum_{k=1}^{N}\left(h^{(k)}/G_{xz}^{(k)}\right)}\,. \tag{3.3}$$

In addition, Ascione et al.[23] extended the theory to the buckling and post-buckling analysis of composite beams particularising the von Kármán kinematic equations to beam structures, and a finite element solution of the RZT nonlinear equilibrium equations is derived using the RZT-C^0 beam finite elements.[37] In the RZT-FE model, the kinematic variables contained in the vector $\mathbf{u}$ are approximated as follows:

$$\mathbf{u} = \begin{Bmatrix} u(x) \\ w(x) \\ \theta(x) \\ \psi(x) \end{Bmatrix} \simeq \mathbf{N}\mathbf{u}^{\mathbf{e}}\,, \tag{3.4}$$

where $\mathbf{u}^{\mathbf{e}}$ is a vector containing the degrees of freedom of the RZT finite element $\mathbf{e}$,

$$\mathbf{u}^{\mathbf{e}} \equiv \begin{bmatrix} u_1 & w_1 & \theta_1 & \psi_1 & u_2 & w_2 & \theta_2 & \psi_2 \end{bmatrix}^T\,, \tag{3.5}$$

and $\mathbf{N}$ is the shape function matrix:

$$\mathbf{N} \equiv \begin{bmatrix} N_1^L & 0 & 0 & 0 & N_2^L & 0 & 0 & 0 \\ 0 & N_1^L & -l^e N_m^Q & -l^e r N_m^Q & 0 & N_2^L & l^e N_m^Q & l^e r N_m^Q \\ 0 & 0 & N_1^L & 0 & 0 & 0 & N_2^L & 0 \\ 0 & 0 & 0 & N_1^L & 0 & 0 & 0 & N_2^L \end{bmatrix}\,, \tag{3.6}$$

where $l^e = L^e/8$ and $r \equiv -(\bar{G} - G)/\bar{G}$, with $\bar{G}$ defined in the Appendix. The functions N_i^L are the linear Lagrange polynomials, whereas N_m^Q is one of the second quadratic Lagrange polynomials (see the Appendix for the complete definitions of these functions). The approximation defined by Eqs.[3.4-3.6] is called *anisoparametric* because the transversal displacement, $w(x)$, is approximated by a quadratic function, whereas linear functions are used for the other kinematic variables. In addition, the constraining condition of a constant transverse-shear force resultant along the element length ($V_{x,x} = 0$) allows a quadratic approximation of $w(x)$ considering a finite element with two nodes only. For this reason, the *anisoparametric-constrained* RZT beam finite element has two nodes and four degrees of freedom per node, as shown in Fig.[5].[37]

The nonlinear FE equilibrium equation for a composite or a sandwich beam, in a perfect configuration (no geometric imperfections), with simply-supported boundary conditions and subjected to an axial-compressive load N_0 (refer to Fig.[6]) is

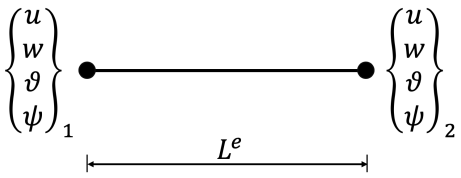

Fig. 5: Two-node constrained anisoparametric element based on the Refined Zigzag Theory for beams.

$$(\mathbf{K} - N_0\mathbf{K_G}) \cdot \mathbf{u} = \mathbf{F}\,, \tag{3.7}$$

where $\mathbf{K}$ is the beam stiffness matrix, $\mathbf{K_G}$ is the geometric stiffness matrix which derives from the geometric nonlinearities, $\mathbf{u}$ is the vector of the degrees of freedom and $\mathbf{F}$ is the vector of the external forces. The definition of these matrices can be found in the Appendix.

Fig. 6: Load and boundary conditions of the beams for the numerical analysis.

The stability equation is obtained employing the Euler's method of the adjacent equilibrium configurations:[39]

$$(\mathbf{K} - N_i\mathbf{K_G}) \cdot \hat{\mathbf{u}}_\mathbf{i} = 0\,, \tag{3.8}$$

where the eigenvalues N_i are discrete values of the applied compressive load N_0 corresponding to the buckling loads of the beam; the eigenvectors, $\hat{\mathbf{u}}_\mathbf{i}$, represent the buckling mode shapes.

3.2. *Numerical evaluation of the critical buckling loads*

The critical buckling loads of the sandwich beams were calculated numerically solving Eq.[3.8] for the RZT-FE models. A similar equation was solved to find the critical buckling loads of the beams for the TBT-FE models. A number of 40 beam finite elements was considered because it was the minimum number of finite elements which could guarantee a convergent solution to that obtained by higher-density

meshes for all the beams. The material properties considered for the numerical analyses are shown in Table [2].

Table 2: Material properties of the sandwich beams.

CFRP-VTM264		**Rohacell®IG31**		**Rohacell®WF110**		**3M™ AF163-2K**	
$\mathbf{E_1}$ (MPa)	120,000	**E** (MPa)	40.3	**E** (MPa)	196	**E** (MPa)	1,100
$\mathbf{E_2}$ (MPa)	7,500	**G** (MPa)	12.5	**G** (MPa)	64.2	**G** (MPa)	400
$\mathbf{E_3}$ (MPa)	7,500						
$\mathbf{G_{12}}$ (MPa)	3,900						
$\mathbf{G_{13}}$ (MPa)	3,900						
$\mathbf{G_{23}}$ (MPa)	2,300						
$\boldsymbol{\nu_{12}}$	0.32						
$\boldsymbol{\nu_{13}}$	0.16						

The properties of AF163-2K indicated that the adhesive was much stiffer than the foams used for the core. In order to investigate the effect of the adhesive on the critical buckling loads, the numerical analyses were performed for both the actual beams with the adhesive material between the core and the facesheets, and for beams without the adhesive layers[a]. Table [3] reports the results of the RZT and the TBT finite element models for both cases, indicating with $\mathrm{N_{cr}^{RZT_{na}}}$ and $\mathrm{N_{cr}^{TBT_{na}}}$ the solutions for the beams where the adhesive was not considered. The shear correction factor used in TBT models was calculated as proposed by Madabhusi-Raman et al.,[15] thus it changed depending on the beam lamination. In Table [3], the percentage difference between the results of the actual beams and those without the adhesive, indicated as $\Delta_\mathrm{R} = (\mathrm{N_{cr}^{RZT}} - \mathrm{N_{cr}^{RZT_{na}}})/\mathrm{N_{cr}^{RZT_{na}}} \cdot 100$ for RZT and $\Delta_\mathrm{T} = (\mathrm{N_{cr}^{TBT}} - \mathrm{N_{cr}^{TBT_{na}}})/\mathrm{N_{cr}^{TBT_{na}}} \cdot 100$ for TBT, depended on the beam properties and on the theory considered for the analysis. The increment of critical buckling load due to the adhesive layers was very small for WF-1-L1 and WF-2-L2, but it was considerably higher for the IG- beams, where the highest values of Δ_R exceeded 4% and Δ_T reached 8%. These results showed that the presence of the adhesive affected the TBT results more than RZT, but also demonstrated that even small layers of adhesive could significantly increase the stiffness and, consequently, the critical buckling load of soft core sandwich beams.

The comparison between the RZT and the TBT solution was done only for the beams with the adhesive layers, indicating with Δ_RT the percentage deviation of RZT with respect to TBT $\left(\Delta_\mathrm{RT} = (\mathrm{N_{cr}^{RZT}} - \mathrm{N_{cr}^{TBT}})/\mathrm{N_{cr}^{TBT}} \cdot 100\right)$. The two FE models gave almost the same results for the critical buckling loads of both the WF-1-L1 and the WF-1-L2 sandwich beams. For these two beams, the value of Δ_RT was less than 1%. Instead, the RZT predictions were significantly higher than the

[a]The total thickness of each beams was kept the same by increasing the core thickness of a value corresponding to the thickness of the two layers of adhesive.

Table 3: Critical buckling loads calculated by the RZT and the TBT finite element models.

	$\mathbf{N_{cr}^{RZT}}$ (N)	$\mathbf{N_{cr}^{RZT_{na}}}$ (N)	$\mathbf{\Delta_R}$ %	$\mathbf{N_{cr}^{TBT}}$ (N)	$\mathbf{N_{cr}^{TBT_{na}}}$ (N)	$\mathbf{\Delta_T}$ %	$\mathbf{\Delta_{RT}}$ %
WF-1-L1	23,266	23,075	0.83	23,264	23,073	0.83	0.01
WF-1-L2	25,053	24,843	0.85	25,052	24,841	0.85	0.00
IG-2-L1	3,224	3,096	4.13	2,809	2,678	4.90	14.77
IG-4-L1	10,695	10,412	2.71	7,061	6,740	4.76	51.47
IG-4-L2	11,399	10,894	4.64	7,617	7,045	8.11	49.65

TBT values when beams with higher face-to-core thickness ratios were considered. The IG-2-L1 beam had a face-to-core thickness ratio of 0.268 (see h_f/h_c in Table [1]), which was almost 8 times the ratio of the WF-1-L-(1-2) beams, and the critical buckling load calculated with RZT was 14.77% higher than the TBT value. The RZT deviation from TBT further increased for IG-4-L1 and IG-4-L2. These two beams had a face-to-core thickness ratio of 0.680 and the RZT results deviated from the TBT solution of 50%.

These numerical results highlighted the dependence of the numerical predictions on the material and the geometric characteristics of the beams. In the following section, the experimental tests are presented in order to assess the two theories for the calculation of the critical buckling loads of sandwich beams of various geometries and core materials.

4. Experimental evaluation of the critical buckling loads

The experiments were performed at the material testing laboratory of the RMIT University, using the Instron compression testing machine with a load cell of 50 kN. As shown in Fig.[7], compression platens were chosen as fixtures of the machine to guarantee a uniformly distributed compressive load along the beam width. The beams were free to rotate around the lateral direction through the cylindrical supports, and their centroidal axis was aligned with the direction of the load to minimise any possible lateral displacement under compression.

A laser displacement sensor (SICK OD1-B100H50U14) was used to measure the transversal displacement of the point at half-length of the beam. The compressive load was progressively increased in displacement control to prevent the beam breakage. The critical buckling loads were calculated employing the Southwell method, thus both the value of the applied load and the transversal displacement of the beam were recorded during the tests. Figs.[8a-12a] show the load-displacement equilibrium paths of the beams obtained by plotting the applied load as a function of transversal displacement at each time step. The test was repeated three times, thus three load-displacement curves were obtained for each beam.

The Southwell plots are reported in Figs.[8b-12b], where the transversal dis-

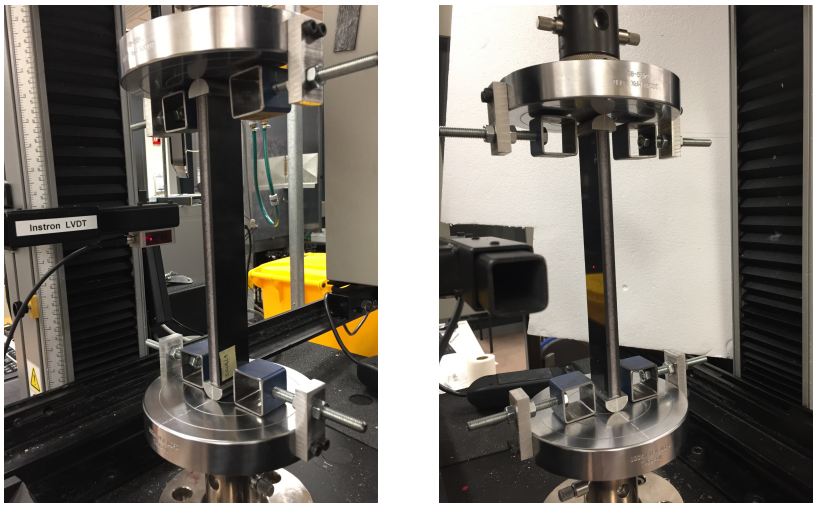

(a) (b)

Fig. 7: Experimental setup for the buckling tests.

placement, w, is plotted as a function of the ratio between w and the corresponding applied load N_0 at each time step. These curves contain only the values of N_0 higher than 80% the maximum applied load and the corresponding transversal displacement values recorded during the experiments.[26]

The experimental curves in the $(w, \frac{w}{N_0})$ plane (Figs.[8b-12b]) were approximated employing the least square method and the slopes of the straight lines were assumed as critical buckling loads.

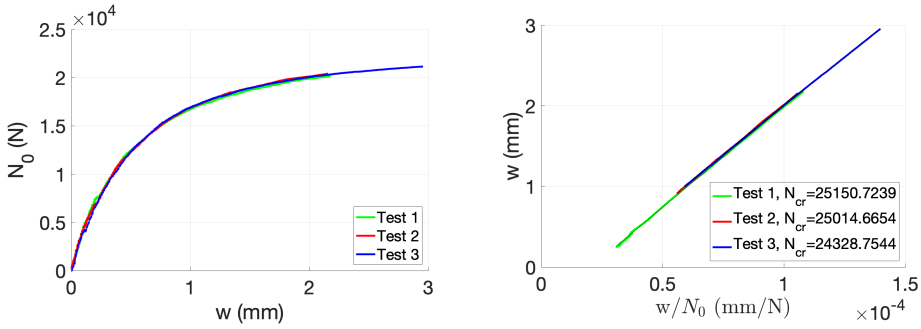

(a) Load-displacement equilibrium path. (b) Southwell plot.

Fig. 8: Experimental evaluation of the critical buckling load of the WF-1-L1 beam.

The equilibrium paths of the WF-1-L1 and WF-1-L2 beams in Figs.[8a-9a] indicate a linear relation between the load and the transversal displacement for low

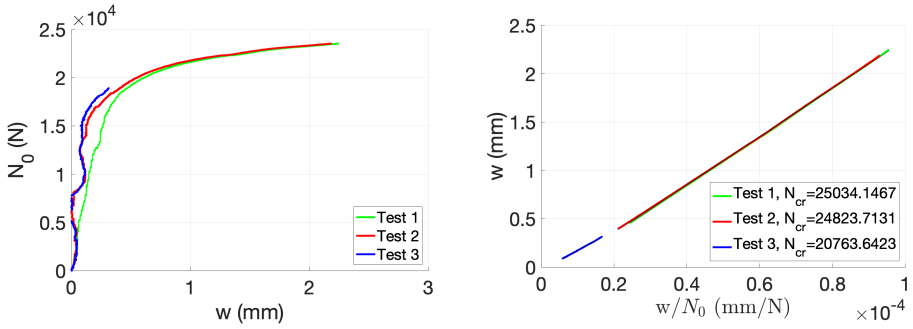

(a) Load-displacement equilibrium path. (b) Southwell plot.

Fig. 9: Experimental evaluation of the critical buckling load of the WF-1-L2 beam.

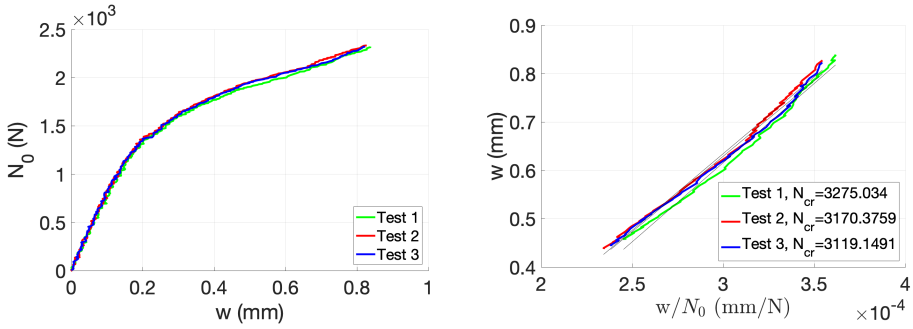

(a) Load-displacement equilibrium path. (b) Southwell plot.

Fig. 10: Experimental evaluation of the critical buckling load of the IG-2-L1 beam.

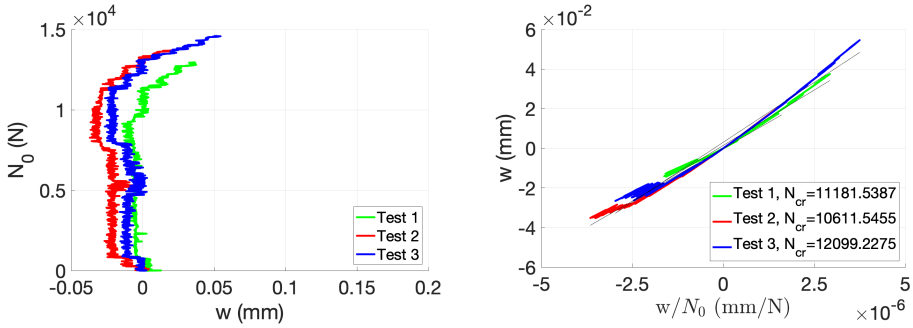

(a) Load-displacement equilibrium path. (b) Southwell plot.

Fig. 11: Experimental evaluation of the critical buckling load of the IG-4-L1 beam.

values of N_0. The slope of the curves rapidly decreases when N_0 exceeds 12,000 N for WF-1-L1 and 17,000 N for WF-1-L2, both having an asymptotic load value of

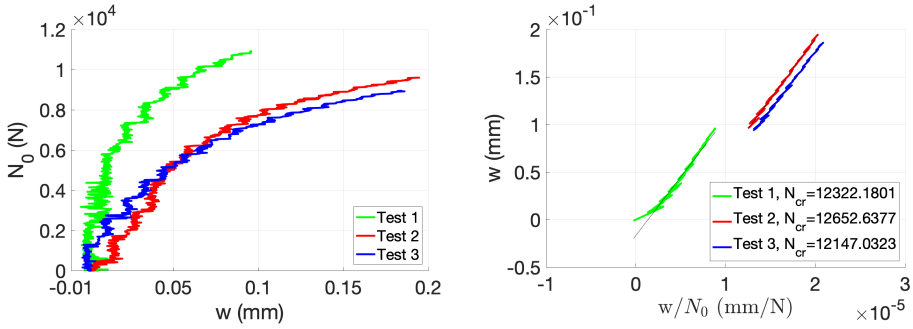

(a) Load-displacement equilibrium path. (b) Southwell plot.

Fig. 12: Experimental evaluation of the critical buckling load of the IG-4-L2 beam.

about 25,000 N. In Fig.[9a], the curve corresponding to the Test 3 of WF-1-L2 ends when the applied load is lower than 20,000 N because during the test one of the semi-cylindrical supports at the beam edges debonded and the test was stopped. The reason of this was a possible misalignment between the load direction and the beam axis with a consequent bending moment on the steel element which caused the debonding. A behaviour similar to WF-1-L(1-2), with an initial linear trend and a subsequent decreasing of the curve slope, can be observed in Fig.[10a] for IG-2-L1. The load-displacement curves of IG-4-L1 and IG-4-L2 in Figs.[11a-12a] exhibit some disturbances due to the high stiffness of the beams. The face-to-core thickness ratio of these beams is very high and their equilibrium paths are very close to the axis $w = 0$. To preserve the beams from breaking, the tests of IG-4-L(1-2) were stopped for very small values of deflection. Indeed, for IG-4-L1, the applied load exceeds the RZT prediction of the critical buckling load for values of w lower than 0.05 mm, whereas in case of IG-4-L2, N_0 is very close to the RZT critical value for w lower than 0.2 mm.

Table 4: Comparison between the experimental and the numerical critical buckling loads.

	$\mathbf{N_{cr}^{EXP}}$ (N)	$\boldsymbol{\sigma}$ (N)	**CV** %	$\mathbf{N_{cr}^{RZT}}$ (N)	**ERR** %	$\mathbf{N_{cr}^{TBT}}$ (N)	**ERR** %
WF-1-L1	24,831	440	1.77	23,266	-6.30	23,264	-6.31
WF-1-L2	24,929	2,407	10.23	25,053	0.50	25,052	0.49
IG-2-L1	3,188	79	2.49	3,224	1.13	2,809	-11.89
IG-4-L1	11,297	750	6.64	10,695	-5.33	7,061	-37.50
IG-4-L2	12,374	256	2.07	11,399	-7.88	7,617	-38.44

In Table [4], the mean value of the buckling loads calculated applying the Southwell method to the experimental data, N_{cr}^{EXP}, was taken as the experimental critical

buckling load of the beams. The WF-1-L2 beam was damaged during Test 3, thus the average critical buckling load reported in Table [4] is the mean between the results of Test 1 and Test 2 only. The standard deviation of the experimental values, σ, and the coefficient of variation, CV, are also indicated.

The values of Δ_{RT} in Table [3] indicate that RZT and TBT provide almost the same results for WF-1-L(1-2). As a consequence, the numerical results of both the FE models have a very similar percentage error with respect to the experimental results of these two beams (see Table [4]). The numerical predictions are excellent for the WF-1-L2 beam, with the RZT and TBT errors lower than 1%. For WF-1-L1, the numerical analysis describes a slightly softer behaviour than the actual beam response detected during the experiments. In this case, the percentage errors of RZT and TBT have negative values and reach -6.30% and -6.31% respectively. However, the TBT error is considerably higher for the remaining beams. It almost reaches -12% for IG-2-L1, whose facesheet thickness is twice the facesheet thickness of WF-1-L(1-2), and goes up to -40% for IG-4-L(1-2), which have a facesheet thickness twice the facesheet thickness of IG-2-L1. On the other hand, the RZT buckling loads are very accurate in all cases. The RZT percentage error is only 1.13% for IG-2-L1 and, for the most challenging situations of beams with a relatively high face-to-core thickness ratio and a highly heterogeneous lamination, as for IG-4-L(1-2), the error is -5.33 and -7.88%, which are excellent results for experimental characterisations.

These results prove the general accuracy of RZT, which is very precise for any kind of beam, and also draw attention to the range of validity of TBT, which is highly inaccurate for some of the beams studied. Moreover, the negative sign of the highest values of error further confirms the importance of modelling the adhesive layers in the numerical analyses. The critical buckling loads of the beams where the adhesive is neglected (see Table [3]) are lower than the RZT and TBT results reported in Table [4], therefore the percentage error with respect to the experimental results would be higher for the beams without the adhesive.

5. Relationship between the numerical predictions and the properties of sandwich beam

In the previous section, the comparison between the numerical predictions and the experimental results showed that RZT was generally very accurate, whereas the TBT error reached very high values for some of the beams investigated. The beams with the highest TBT error were those with higher face-to-core thickness ratios, h_f/h_c, and a higher difference between the material properties of the facesheets and the core. The heterogeneity level of the beam lamination can be expressed as the ratio between the Young's moduli of the facesheet and the core, E_f/E_c. In this section it is shown that the face-to-core thickness ratio and the face-to-core stiffness ratio can significantly influence the TBT results and its difference from RZT.

A parametric study was conducted to determine the relationship between the

TBT deviation from RZT and the geometrical and material properties of a sandwich beam for calculating the critical buckling load.

Seven sandwich beams with CFRP-VTM264 facesheets (material properties indicated in Table [2]) and a foam core were considered in the analysis. Each facesheet had 4 layers with a $[0°/90°/90°/0°]$ fibre orientation and a thickness value h_f reported in Table [5]. The same slenderness ratio, $L/h = 20$, was considered for all the beams and the width, b, was three times the total thickness h. The C20F(08-16-32) beams had the same core thickness, $h_c = 20$ mm, whereas the facesheets were, respectively, 0.8 mm, 1.6 mm and 3.2 mm thick. The C5F(08-16-32) beams had a smaller core thickness, $h_c = 5$ mm, but the facesheets were also 0.8 mm, 1.6 mm and 3.2 mm thick, respectively. Table [5] shows that, for the assumed thickness values, the face-to-core thickness ratio, h_f/h_c, gradually increases from 0.04 for the C20F08 beam to 0.64 for the C5F32 beam, and that the beams C20F32, C6F096 and C5F08 have the same h_f/h_c. The Young's modulus of the core, E_c, was considered as a parameter and its value was increased from 10 MPa to 60,000 MPa. The average Young's modulus in the axial direction, $E_f = 64,069$ MPa, was calculated for the multilayer facesheets according to Jones.[40] The face-to-core stiffness ratios obtained for the two limiting values of E_c were $E_f/E_c = 6,406.9$, which corresponded to a sandwich beam with a highly heterogeneous material lamination, and $E_f/E_c = 1.07$, which was a value close to that of an isotropic configuration. The critical buckling loads of the beams were calculated for each value of E_c considered, using both the RZT and the TBT FE models.

Table 5: Thickness values of the beams for the parametric analysis.

	$\mathbf{h_c}$ (mm)	$\mathbf{h_f}$ (mm)	$\mathbf{h_f/h_c}$ -
C20F08	20	0.8	0.04
C20F16	20	1.6	0.08
C20F32	20	3.2	0.16
C6F096	6	0.96	0.16
C5F08	5	0.8	0.16
C5F16	5	1.6	0.32
C5F32	5	3.2	0.64

The deviation of the TBT solution with respect to RZT, $\Delta_{\mathrm{TR}} = (\mathrm{N}_{\mathrm{cr}}^{\mathrm{TBT}} - \mathrm{N}_{\mathrm{cr}}^{\mathrm{RZT}})/\mathrm{N}_{\mathrm{cr}}^{\mathrm{RZT}} \cdot 100$, is shown in Figs.[13] as a function of the face-to-core stiffness ratio. The curves show that Δ_{TR} has very small values when E_f/E_c is close to the limiting condition of an isotropic beam, indicating that the TBT and the RZT models give similar results for the critical buckling load of sandwich beams with very stiff cores. In general, Δ_{TR} fluctuates in the range of small E_f/E_c ratios until it reaches a minimum value for $E_c = \bar{E}_c$. For all the beams, Δ_{TR} never exceeds 0.5% in the range of small E_f/E_c ratios ($E_f/E_c < E_f/\bar{E}_c$), growing almost linearly

for higher face-to-core stiffness ratios. This behaviour is clearly visible in Fig.[13a] for C20F08.

The C20F08 beam has the lowest values of TBT deviation; even for highly heterogeneous material lamination Δ_{TR} does not exceed 0.7%. The results of the C20F(08-16-32) beams in Figs.[13a,13c,13e] indicate that the value of Δ_{TR} rises for higher values of facesheet thickness. As an example, the facesheet thickness of C20F16 is double the value of C20F08 and the TBT deviation is more than five times the corresponding values of the C20F08. Moreover, at the maximum value of face-to-core stiffness ratio considered, Δ_{TR} reaches 4% for C20F16 and 22% for the C20F32 beam. The same behaviour can be noticed comparing the results of the C5F(08-16-32) beams in Figs.[13b,13d,13f], where the TBT deviation as h_f increases. For these beams, Δ_{TR} has significantly higher values than the C20F(08-16-32) beams, being close to 90% for C5F16 and exceeding 200% for C5F32 at the highest E_f/E_c considered.

Table 6: Face-to-core stiffness ratio ($E_f/\bar{E}_c$) and Young's modulus of the core ($\bar{E}_c$) corresponding to the minimum value of Δ_{TR} depending on the thickness ratio of each beam.

	$\mathbf{h_f/h_c}$ -	$\mathbf{E_f/\bar{E}_c}$ -	$\mathbf{\bar{E}_c}$ (MPa)
C20F08	0.04	142.37	450
C20F16	0.08	51.67	1,240
C20F32-C5F08-C6F096	0.16	2.14	30,000
C5F16	0.32	0.58	110,000
C5F32	0.64	0.58	110,000

It is clear that the magnitude of the TBT deviation depends on both the face-to-core stiffness and thickness ratios; moreover, Figs.[13e,13b,13g] demonstrate that beams with the same face-to-core thickness ratio have the exact same trend of Δ_{TR}. In case of very thin facesheets, as for $h_f/h_c < 0.08$ (refer to Fig.[13a]), Δ_{TR} is lower than 1% also for E_f/E_c ratios relatively high. For $h_f/h_c = 0.08$, as C20F16 in Fig.[13c], the TBT deviation is higher than 1% only for $E_c < 30$ MPa, which means it would be lower than 1% even for a soft core made of Rohacell®IG31.

For the beams C20F32, C5F08 and C6F096, which have $h_f/h_c = 0.16$, Δ_{TR} is lower than 1% only for relatively stiff foam cores such as a Rohacell®WF110 (corresponding to $E_f/E_c = 327$), whereas it goes up to 5% for an IG31 core. Considering a bigger h_f/h_c ratio, as C5F16 and C5F32 (Figs.[13d-13f]), the percentage difference between TBT and RZT is significantly high even for stiff cores, reaching 2.6% for C5F16 and 6.5% for C5F32 when the core is made of WF110.

In addition, the thickness ratio influences also the value $E_f/\bar{E}_c$, which diminishes as the face-to-core thickness ratio decreases, as shown in Table [6]. The decrement of $E_f/\bar{E}_c$ implies that Δ_{TR} has a trend that is close to linear in a wider range of

E_f/E_c ratios for beams with higher h_f/h_c ratios.

The linear interpolation of Δ_{TR} for $E_f/E_c > E_f/\bar{E}_c$ is reported in Figs.[14] with the corresponding R^2 value of the fit for each case. The slope of the fitting curve, p, is different for each beam, increasing with h_f/h_c as shown in Fig.[15]. The comparison between Fig.[13a] and Fig.[13f] highlights a major influence on Δ_{TR} of the face-to-core thickness ratio than the stiffness ratio. Indeed, C20F08 has the lowest h_f/h_c ratio and Δ_{TR} does not have significant values even for a highly heterogeneous material laminations. On the other hand, C5F08 has the highest face-to-core thickness ratio and Δ_{TR} reaches high values even for beam with a very low heterogeneity.

This study points out that the heterogeneity of the materials and the thickness of the facesheets and the core affect the accuracy of the TBT prediction of the critical buckling load. The TBT error increases for higher E_f/E_c in a relationship that is close to linear, whereas a higher-order dependance exists between the TBT error and h_f/h_c.

6. Discussion

The experiments demonstrated that RZT is generally very accurate for predicting the critical buckling load of sandwich beams, whereas the error of TBT exceeded 10% for most of the beams considered. The subsequent parametric analysis showed that the percentage deviation of TBT from RZT, Δ_{TR}, increased with both the face-to-core thickness and stiffness ratios. The values of Δ_{TR} and the percentage errors of TBT with respect the experimental results are summarised in Table [7]. They show that the beams with the highest deviation from RZT are those with the highest TBT error in comparison to the experiments and Δ_{TR} and ERR have similar values for those beams. This proves that TBT can be highly inaccurate in some cases, whereas RZT is always very precise instead. Moreover, the beams considered in the parametric analysis have the same slenderness ratio, but it is reasonable to believe that the TBT errors would be higher for lower slenderness ratios.

Table 7: Comparison between the TBT deviation from RZT and the TBT error with respect to the experimental results.

	$\boldsymbol{\Delta}_{\mathrm{TR}}$ %	**ERR** %
WF-1-L1	-0.01	-6.31
WF-1-L2	-0.01	0.49
IG-2-L1	-13.51	-11.89
IG-4-L1	-35.27	-37.50
IG-4-L2	-35.33	-38.44

In general, the numerical methods like FEM can be preferable to experiments for saving time. Indeed, the manufacture of beams investigated in this work and the testing activity can take days to be completed, whereas a numerical buckling analysis requires only few minutes to run. Moreover, routines based on one-dimensional finite elements, like the RZT and the TBT FE models presented in this study, are able to calculate the critical buckling load of sandwich beams in a few seconds. On the other hand, accurate FE models realised with commercial codes, which are the most used technique for structural analysis, can be computationally less efficient than RZT and TBT because they are based on two- or three-dimensional finite elements (one-dimensional models of commercial codes are not generally accurate for composite and sandwich beams). However, TBT has proven not to be accurate enough in general despite its computational efficiency, and previous works showed that one-dimensional models based on RZT finite elements can reach the same level of accuracy of highly detailed FE models realised with commercial codes. Although in many applications sandwiches are realised with very thin facesheets to reduce the weight keeping the stiffness high by adding the core material, and TBT would not have problems in those cases, the aim of this effort is to issue a warning for both present and future designs of sandwich beams, which should take into consideration the limits of TBT for the analysis of sandwich beams, and to propose a method that is generally valid for any lamination and beam geometry.

7. Conclusion

Prior works have shown the numerous advantages of the Refined Zigzag Theory in terms of computational cost and accuracy when employed for the analysis of composite and sandwich beams. However, in these studies the application of the RZT for evaluating the critical buckling loads of composite beams has been only numerically verified through a comparison to highly detailed FE models realised in commercial codes. In this study, five sandwich beams of various geometries and two different foam cores were tested in compression and the Southwell method was employed for calculating the experimental critical buckling loads of the beams in simply-supported boundary conditions. In addition, the nonlinear FE formulation of the RZT, which involved the beam geometric nonlinearities, was applied for calculating the critical buckling loads of the beams based on the RZT. Two FE models were realised for each beam, one based on TBT-beam finite elements and one based on RZT-beam finite elements, and for each model the critical buckling load was calculated. The numerical predictions were assessed comparing them to the results obtained from the experiments. The percentage error of TBT and RZT with respect to the experimental values showed that both numerical models were quite accurate when employed for sandwich beams with thin facesheets and a Rohacell®WF110 foam core. However, the TBT error for the remaining beams was significantly higher, reaching 38%, whereas RZT was generally very accurate, having error lower than 8% in any case.

In addition, a parametric analysis identified a dependance of the TBT error on the beam face-to-core thickness ratio and on the heterogeneity of the materials, that was indicated by the ratio between the Young's moduli of facesheet and core. The TBT error increased almost linearly with the face-to-core stiffness ratio and it also showed a higher-order relationship with the face-to-core thickness ratio. These results confirmed that the accuracy of TBT decreased for highly heterogeneous sandwich beams and for bigger facesheet thicknesses.

To the authors' knowledge, this is the first study where RZT was experimentally assessed for the calculation of the critical buckling load of sandwich beams. The outcomes of the present work highlighted some limits in the applicability of TBT for the calculation of the critical buckling load of sandwich beams and validated all the RZT predictions, even for highly heterogeneous soft-core beams, further confirming the RZT accuracy and superior capabilities with respect to commonly used ESL approaches.

Acknowledgments

The authors would like to thank Mr Paul Muscat and the RMIT technical staff for their support and assistance in the beam manufacture and testing.
The authors acknowledge the RMIT University for supporting this work through a grant.

Appendix A.

The parameter $\bar{G}$ is the average thickness-weighted transverse-shear modulus of the total laminate defined as

$$\bar{G} \equiv \frac{1}{2h} \int_{-h}^{+h} G_{xz}^{(k)} dz \,. \tag{A.1}$$

Introducing the non-dimensional axial coordinate $\xi \equiv 2x/L^e - 1 \in [-1, 1]$, the linear and quadratic Lagrange polynomials are defined as follows:

$$[N_1^L, N_2^L] = \left[\frac{1}{2}(1-\xi), \frac{1}{2}(1+\xi)\right], \tag{A.2}$$

$$[N_1^Q, N_m^Q, N_2^Q] = \left[\frac{1}{2}\xi(\xi-1), (1-\xi^2), \frac{1}{2}\xi(\xi+1)\right]. \tag{A.3}$$

The stiffness matrix and geometric stiffness matrix of the beam in Eqs.[3.7-3.8] ($\mathbf{K}$ and $\mathbf{K_G}$) are obtained by assembling the element-based matrices $\mathbf{K^e}$ and $\mathbf{K_G^e}$, which are defined as

$$\mathbf{K^e} \equiv \int_{x_a}^{x_b} \mathbf{B^e}^T \left[\int_A \left(\mathbf{Z_\epsilon}^{(k)T} E_x^{(k)} \mathbf{Z_\epsilon}^{(k)} + \mathbf{Z_\gamma}^{(k)T} G_{xz}^{(k)} \mathbf{Z_\gamma}^{(k)} \right) dA \right] \mathbf{B^e} dx \,, \tag{A.4}$$

$$\mathbf{K_G^e} \equiv \int_{x_a}^{x_b} \mathbf{B^e}^T \mathbf{H} \mathbf{B^e} dx \,, \tag{A.5}$$

$$\tag{A.6}$$

where $\mathbf{B^e}$ is the matrix containing the derivatives of the shape functions with respect to the x coordinate,

$$\mathbf{B^e} \equiv \begin{bmatrix} N_{1,\xi}^L & 0 & 0 & 0 & N_{2,\xi}^L & 0 & 0 & 0 \\ 0 & N_{1,\xi}^L & -l^e N_{m,\xi}^Q & -l^e c N_{m,\xi}^Q & 0 & N_{2,\xi}^L & l^e N_{m,\xi}^Q & l^e c N_{m,\xi}^Q \\ 0 & 0 & L^e N_1^L & 0 & 0 & 0 & L^e N_2^L & 0 \\ 0 & 0 & 0 & L^e N_1^L & 0 & 0 & 0 & L^e N_2^L \\ 0 & 0 & N_{1,\xi}^L & 0 & 0 & 0 & N_{2,\xi}^L & 0 \\ 0 & 0 & 0 & N_{1,\xi}^L & 0 & 0 & 0 & N_{2,\xi}^L \end{bmatrix} , \tag{A.7}$$

The matrices $\mathbf{Z_\epsilon^{(k)}}$ and $\mathbf{Z_\gamma^{(k)}}$ are

$$\mathbf{Z_\epsilon}^{(k)} = \begin{bmatrix} 1 & 0 & 0 & 0 & z & \phi^{(k)} \end{bmatrix} , \tag{A.8}$$

$$\mathbf{Z_\gamma}^{(k)} = \begin{bmatrix} 0 & 1 & 1 & \beta^{(k)} & 0 & 0 \end{bmatrix} , \tag{A.9}$$

and $\mathbf{H}$ is the following zero-one matrix:

$$\mathbf{H} = \begin{bmatrix} 0 & 0 & 0 & 0 & 0 & 0 \\ 0 & 1 & 0 & 0 & 0 & 0 \\ 0 & 0 & 0 & 0 & 0 & 0 \\ 0 & 0 & 0 & 0 & 0 & 0 \\ 0 & 0 & 0 & 0 & 0 & 0 \\ 0 & 0 & 0 & 0 & 0 & 0 \end{bmatrix} . \tag{A.10}$$

References

1. H. F. Seibert, Applications for PMI foams in aerospace sandwich structures, *Reinf. Plast.* **50**(1) (2006) 44–48.
2. R. Krämer and M. A. Roth, Experimental and numerical analysis of hollow and foam-filled A- stringer/A-former under axial compression load and bending moment, *J. Sandw. Struct. Mater.* **9**(2) (2007) 197–208.
3. S. P. Timoshenko, On the correction for shear of differential equations for transverse vibrations of prismatic bars, *Lond. Edinb. Dubl. Phil. Mag.* **41**(245) (1921) 744–746.
4. S. P. Timoshenko, X. On the transverse vibrations of bars of uniform cross-section, *Lond. Edinb. Dubl. Phil. Mag. J. Sci.* **43**(253) (1922) 125–131.
5. Y. Frostig, M. Baruch, O. Vilnay and I. Sheinman, High-order theory for sandwich-beam behavior with transversely flexible core, *J. Eng. Mech.* **118**(5) (1992) 1026–1043.
6. Y. Frostig and M. Baruch, High-order buckling analysis of sandwich beams with transversely flexible core, *J. Eng. Mech.* **119**(3) (1993) 476–495.
7. A. A. Khdeir and J. N. Reddy, An exact solution for the bending of thin and thick cross-ply laminated beams, *Compos. Struct.* **37**(2) (1997) 195–203.
8. A. A. Khdeir and J. N. Reddy, Buckling of cross-ply laminated beams with arbitrary boundary conditions, *Compos. Struct.* **37**(1) (1997) 1–3.
9. A. A. Khdeir and J. N. Reddy, Free vibration of cross-ply laminated beams with arbitrary boundary conditions, *Int. J. Eng. Sci.* **32**(12) (1994) 1971–1980.
10. M. A. Ramos Loja, J. Infante Barbosa and C. M. Mota Soares, Static and dynamic behaviour of laminated composite beams, *Int. J. Struct. Stab. Dyn.* **1**(4) (2001) 545–560.
11. D. Liu and X. Li, An overall view of laminate theories based on displacement hypothesis, *J. Compos. Mater.* **30**(14) (1996) 1539–1561.
12. V. Kahya, Buckling analysis of laminated composite and sandwich beams by the finite element method, *Compos. Part B-Eng.* **91** (2016) 126–134.
13. D. H. J. Robbins and J. N. Reddy, Modeling of thick composites using a layer-wise theory, *Int. J. Numer. Meth. Eng.* **36**(4) (1993) 337–343.
14. M. Tahani, Analysis of laminated composite beams using layerwise displacement theories, *Compos. Struct.* **79**(4) (2007) 535–547.
15. P. Madabhusi-Raman and J. F. Davalos, Static shear correction factor for laminated rectangular beams, *Compos. Part B-Eng.* **27**(3) (1996) 285–293.
16. M. Di Sciuva, Bending, vibration and buckling of simply supported thick multilayered orthotropic plates: an evaluation of a new displacement model, *J. Sound Vib.*. **105**(3) (1986) 425-442.
17. R. P. Khandelwal, A. Chakrabarti and P. Bhargava, Vibration and buckling analysis of laminated sandwich plate having soft core, *Int. J. Struct. Stab. Dyn.* **13**(8) (2013) 1350034.
18. A. Tessler, M. Di Sciuva and M. Gherlone, A refined zigzag beam theory for composite and sandwich beams, *J. Compos. Mater.* **43** (2009) 1051–1081.
19. L. Iurlaro, M. Gherlone, M. Di Sciuva and A. Tessler, Assessment of the refined zigzag theory for bending, vibration, and buckling of sandwich plates: a comparative study of different theories, *Compos. Struct.* **106** (2013) 777–792.
20. L. Iurlaro, M. Gherlone and M. Di Sciuva, Bending and free vibration analysis of functionally graded sandwich plates using the refined zigzag theory, *J. Sandw. Struct. Mater.* **16** (2014) 669–699.
21. L. Iurlaro, M. Gherlone, M. Mattone and M. Di Sciuva, Experimental assessment of the refined zigzag theory for the static bending analysis of sandwich beams, *J. Sandw. Struct. Mater.* **20** (2018) 86–105.
22. L. Iurlaro, A. Ascione, M. Gherlone, M. Mattone and M. Di Sciuva, Free vibration

analysis of sandwich beams using the refined zigzag theory: an experimental assessment, *Meccanica*. **50** (2015) 2525–2535.
23. A. Ascione and M. Gherlone, Nonlinear static response analysis of sandwich beams using the refined zigzag theory, *J. Sandw. Struct. Mater.* (2018) DOI:10.1177/1099636218795381.
24. R. V. Southwell, On the analysis of experimental observations in problems of elastic stability, in *Proc. of the Royal Society London Series A*, (April 1932) vol. 135, pp. 601–616.
25. A. Chailleux, Y. Hans and G. Verchery, Experimental study of the buckling of laminated composite columns and plates, *Int. J. Mech. Sci.* **17**(8) (1975) 489–498.
26. J. Singer, J. Arbocz and T. Weller, *Buckling Experiments: Experimental Methods in Buckling of Thin-Walled Structures: Basic Concepts, Columns, Beams and Plates* (John Wiley & Sons, 2007).
27. L. H. Donnell, *On the application of Southwell's method for the analysis of buckling tests*, S. Timoshenko 60th Anniversary Volume, pp. 27–38 (McGraw-Hill, New York, 1938).
28. W. T. Tsai, Note on Southwell's method for buckling tests of struts, *J. Appl. Mech.* **53**(4) (1986) 953–954.
29. E. E. Lundquist, Generalized analysis of experimental observations in problems of elastic stability, Report NACA, Technical Note 658 (1938).
30. P. Mandal and C. Calladine, Lateral-torsional buckling of beams and the Southwell plot, *Int. J. Mech. Sci.* **44**(12) (2002) 2557–2571.
31. H. B. Blum and K. J. R. Rasmussen, Elastic buckling of columns with a discrete elastic torsional restraint, *Thin-Walled Struct.* **129** (2018) 502–511.
32. T. T. Nguyen, T. M. Chan and J. T. Mottram, Lateral-torsional buckling resistance by testing for pultruded FRP beams under different loading and displacement boundary conditions, *Compos. Part B-Eng.* **60** (2014) 306–318.
33. J. Belis, C. Bedon, C. Louter, C. Amadio and R. Van Impe, Experimental and analytical assessment of lateral torsional buckling of laminated glass beams, *Eng. Struct.* **51** (2013) 295– 305.
34. L. Valarinho, J. R. Correia, M. Machado-e-Costa, F. A. Branco and N. Silvestre, Lateral- torsional buckling behaviour of long-span laminated glass beams: Analytical, experimental and numerical study, *Mater. Design.* **102** (2016) 264–275.
35. V. P. Veedu and L. A. Carlsson, Finite-element buckling analysis of sandwich columns containing a face/core debond, *Compos. Struct.* **69**(2) (2005) 143–148.
36. H. Mahfuz, S. Islam, M. Saha, L. Carlsson and S. Jeelani, Buckling of sandwich composites; effects of core–skin debonding and core density, *Appl. Compos. Mater.* **12**(2) (2005) 73–91.
37. M. Gherlone, A. Tessler and M. Di Sciuva, C0 beam elements based on the refined zigzag theory for multilayered composite and sandwich laminates, *Compos. Struct.* **93** (2011) 2882–2894.
38. A. Ascione, *Synthetic models for the analysis and control of composite and sandwich aerospace structures in critical conditions*, PhD Thesis, Politecnico di Torino-RMIT University (2019).
39. D. O. Brush and B. O. Almroth, *Buckling of bars, plates and shells*, (McGraw-Hill, 1975).
40. R. M. Jones, *Mechanics of composite materials*, CRC press (2014).

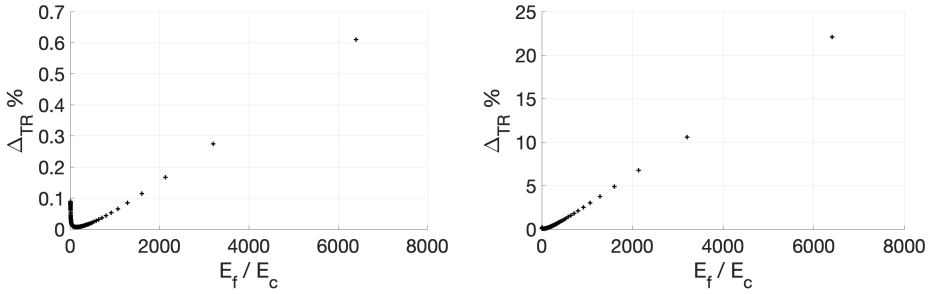

(a) C20F08, $h_f/h_c = 0.04$.

(b) C5F08, $h_f/h_c = 0.16$.

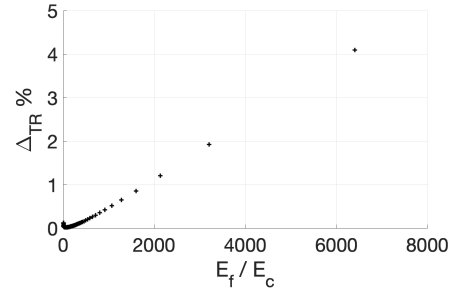

(c) C20F16, $h_f/h_c = 0.08$.

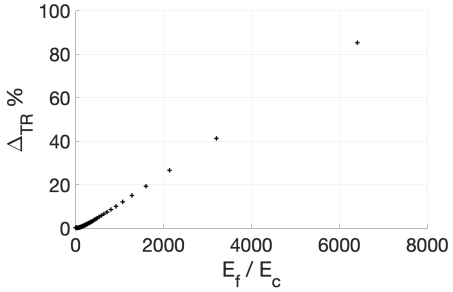

(d) C5F16, $h_f/h_c = 0.32$.

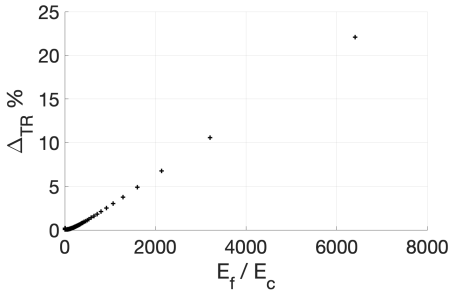

(e) C20F32, $h_f/h_c = 0.16$.

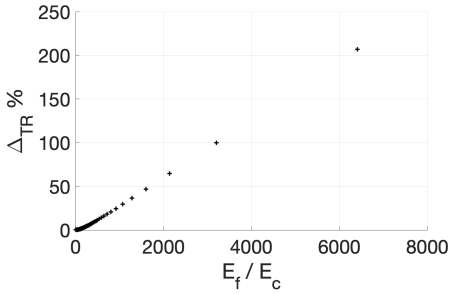

(f) C5F32, $h_f/h_c = 0.64$.

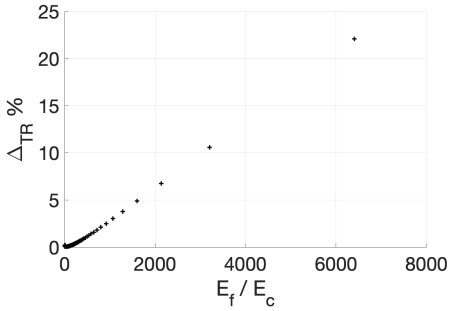

(g) C6F096, $h_f/h_c = 0.16$.

Fig. 13: Percentage deviation of the TBT critical buckling load from RZT as a function of the face-to-core stiffness ratio for beams with various thickness values.

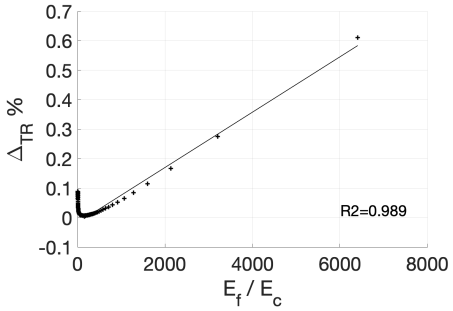

(a) C20F08, $h_f/h_c = 0.04$.

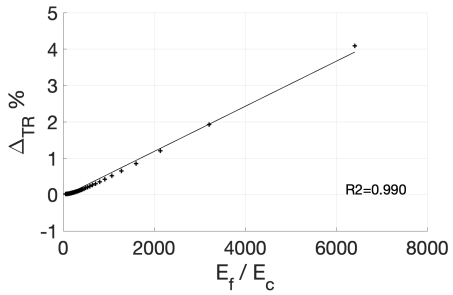

(b) C20F16, $h_f/h_c = 0.08$.

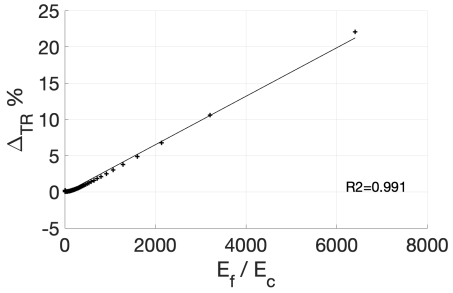

(c) C20F32, C5F08 and C6F096, $h_f/h_c = 0.16$.

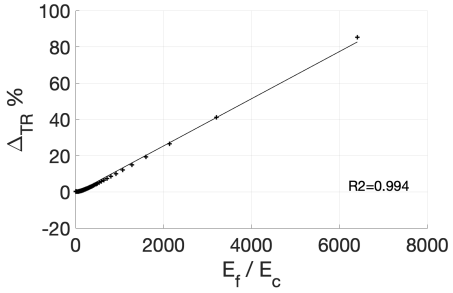

(d) C5F16, $h_f/h_c = 0.32$.

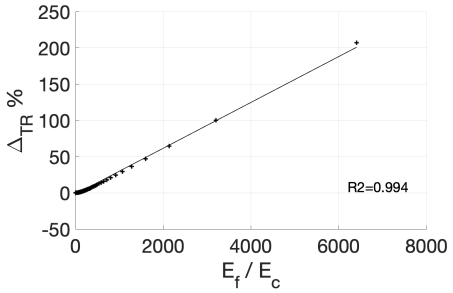

(e) C5F32, $h_f/h_c = 0.64$.

Fig. 14: Linear fit of Δ_{TR} for $E_f/E_c > E_f/\bar{E}_c$.

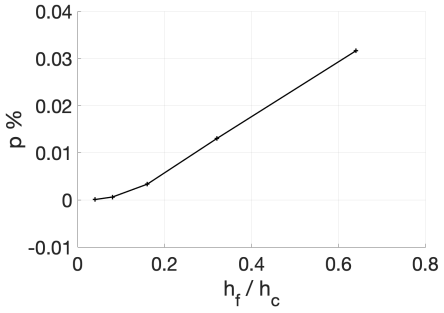

Fig. 15: Slope of the fitting curves of Figs.[14] as a function of the face-to-core thickness ratio.